Molecular Crystals and Liquid Crystals

Publication details, including instructions for authors and subscription information:
http://www.tandfonline.com/loi/gmcl20

On the Importance of the Molecular Core Interactions on the Induction of the High Optical Tilt Angle

W. Piecek [a], Z. Raszewski [a], P. Perkowski [a], J. Kędzierski [a], J. Rutkowska [a], E. Nowinowski-Kruszelnicki [a], J. Zieliński [a], R. Dąbrowski [b] & X. W. Sun [c]

[a] Institute of Applied Physics, Military University of Technology, Warszawa, Poland

[b] Institute of Chemistry, Military University of Technology, Warszawa, Poland

[c] School of Electrical & Electronic Engineering, Nanyang Technological University, Nanyang, Singapore

Version of record first published: 22 Sep 2010

To cite this article: W. Piecek, Z. Raszewski, P. Perkowski, J. Kędzierski, J. Rutkowska, E. Nowinowski-Kruszelnicki, J. Zieliński, R. Dąbrowski & X. W. Sun (2007): On the Importance of the Molecular Core Interactions on the Induction of the High Optical Tilt Angle, Molecular Crystals and Liquid Crystals, 477:1, 205/[699]-221/[715]

To link to this article: http://dx.doi.org/10.1080/15421400701732431

Mol. Cryst. Liq. Cryst., Vol. 477, pp. 205/[699]–221/[715], 2007

ISSN: 1542-1406 print/1563-5287 online
DOI: 10.1080/15421400701732431

On the Importance of the Molecular Core Interactions on the Induction of the High Optical Tilt Angle

W. Piecek
Z. Raszewski
P. Perkowski
J. Kędzierski
J. Rutkowska
E. Nowinowski-Kruszelnicki
J. Zieliński
Institute of Applied Physics, Military University of Technology, Warszawa, Poland

R. Dąbrowski
Institute of Chemistry, Military University of Technology, Warszawa, Poland

X. W. Sun
School of Electrical & Electronic Engineering, Nanyang Technological University, Nanyang, Singapore

Two smectogens being structural analogs with the opposite space orientation of the COO ester group in the molecular core exhibit extremely different tilt angles. A molecular mechanism of the induction of the high optical tilt angle is searched on the basis of extensive investigations of those compounds.

Computer modeling of molecules and investigations of physical parameters of smectic phases were done. Different molecular aggregates forming smectic phases were observed. The size and shape of those aggregates are estimated on the basis of

We would like to express our great gratitude to dr. A. Bubnov (Institute of Physics Academy of Sciences of the Czech Republic, Na Slovance 2, Praha, Czech Republic) for help in SAXS measurements and fruitful discussions. We appreciate our cooperation with M.Sc., M. Filipowicz (Institute of Chemistry of Military University of Technology) for DSC measurements. The project has been supported witch funds of Polish Ministry of Science and Higher Education for years 2006–2009 under KBN grant no.: Singapore/13/2006 (Grant WAT SPG 29041/WAT/2006).

Address correspondence to Wiktor Piecek, Institute of Applied Physics, Military University of Technology, ul. Kaliskiego Str. 2, 00-908 Warszawa, Poland. E-mail: wpiecek@wat.edu.pl

measurements and calculations. The different values of the tilt angles in studied compounds were discussed.

Keywords: de Vries SmA* phase; dimmerisation; orthoconic smectic phases; smectic liquid crystals; tilt angle

1. INTRODUCTION

Looking for a mechanism of induction of orthoconic smectic phase two well known [1–3], mesogenic compounds: 4′octyloxy-biphenyl-4-carboxylic acid 4-(1-methyl-heptyloxy)-phenyl

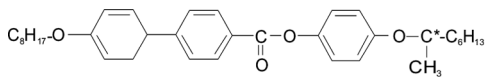

(in short called CO-20)

and 4-(1-methyl-heptyloxy)-benzioc acid 4′-octyloxy-biphenyl-5-yl ester

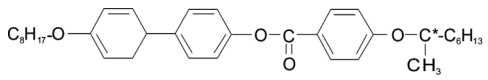

(in short called OC-45)

were investigated by means of electrooptical, dialectical and X-ray measurements.

It should be noted that the only structural difference between them is the orientation of the ester COO group located in the same place of the molecular rigid core. The small change in the structure of molecules causes huge differences in mesogenic phases created by them. The other, most important difference, is a molecular tilt angles in SmC* phases. The compound of CO-20 has got small tilt angle while the OC-45 one exhibits high optical tilt. It is worth emphasizing that the OC-45 compound is a rare example of tilted smectic which exhibits 45° tilt angle with almost thermal independent characteristics. The main aim of presented study is to learn out the nature of creation of high (orthoconic) and small tilted smectic phases.

2. THE EXPERIMENT AND THE RESULTS

A number of structural and physical parameters were studied by standard methods [4]. The tilt angles θ, spontaneous polarizations P_s, switching times τ and rotational viscosity γ were investigated using specially prepared in our laboratory the 1.6 [μm] thick cells filled with material under study in isotropic phases by capillary actions. Cell surfaces were coated by PI2610 (DuPont) polyimide and followed by

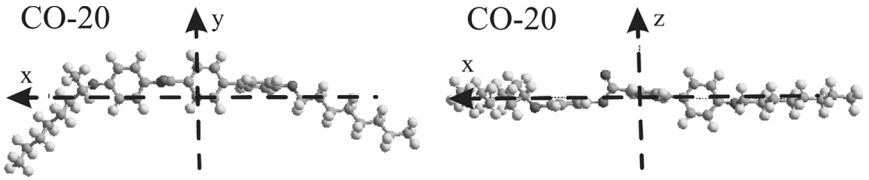

FIGURE 1 The picture of the estimated molecular conformation of compound CO-20.

suitable antiparallel rubbing. The uniform quasi-bookshelf structures were obtained during several slow melting-cooling cycles ($\sim$0.05 [°C/min]) in the presence of the electric field ($E \approx 12$ [V/μm]). All measurements were performed upon cooling from the isotropic (Iso) phases. The cooling rate was about 0.01 [°C/min].

2.1. Computer simulation

To find the shapes and functional dimensions of CO-20 and OC-45 molecules Hyper Chem. 5.0 molecular modeling software were used with molecular mechanics method MM+ and semi-empirical method MNDO. Consequently, the most favorable end-to-end length l_{20} for CO-20 and l_{45} (in gas state) for OC-45 as well as the fully extended one l_{20}^{m}, l_{45}^{m} were estimated. Furthermore, the μ_x, μ_y, μ_z components of molecular dipole moments in the local Oxyz system of coordinates were obtained. The Ox, axis of this local system connected with a molecule, was collinear with the longest axis of inertia ellipsoid of revolution of the single molecule. The Oz axis of local system of coincidences was collinear with the shortest axis of inertia ellipsoid of revolution of the single molecule.

Calculated results of the computer simulation for the CO-20 and OC-45 are presented in the Figures 1 and 2 and gathered in the Table 1.

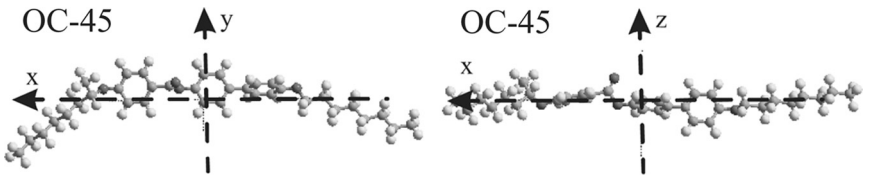

FIGURE 2 The picture of the calculated molecular conformation of compound OC-45.

TABLE 1 Calculated Molecular Parameters of CO-20 and OC-45 Compounds

	Molecular Length [Å]	β	Dipole moment [D]					φ	γ
			μ_x	μ_y	μ_z	μ	$\mu_\perp$		
CO-20	$l_{20} = 34.3$ $l_{20}^m = 37.0$	$\beta_{20} = 167.8^\circ$	−0.09	1.92	−0.99	$\mu^{20} = 2.16$	$\mu_\perp^{20} = 2.16$	$\varphi_{20} = -63^\circ$	$\gamma_{20} = 90$
OC-45	$l_{45} = 35.1$	$\beta_{45} = 168.8^\circ$	−0.22	1.98	1.67	$\mu^{45} = 2.60$	$\mu_\perp^{45} = 2.59$	$\varphi_{45} = +50^\circ$	$\gamma_{45} = 90^\circ$

μ – the magnitude of the molecular dipole moment $\vec{\mu}$,
μ_x, μ_y, μ_z-the x, y, z components of the molecular dipole moment $\vec{\mu}$,
$\mu_\perp$ – the perpendicular component of the dipole moment $\vec{\mu}$
φ – the angle between the dipole moment $\vec{\mu}$ and short Oz molecular axis,
γ – the angle between the dipole moment $\vec{\mu}$ and long Ox molecular axis,
β – the angle between rigid molecular core and the chiral part.

2.2. Transition Temperatures and Enthalpies

Table 1 shows transition temperatures and enthalpies for CO-20 and OC-45 compounds. The phase transition temperatures and enthalpies were determined by differential scanning calorimetry (DSC), using a SETARAM 141 instrument. Liquid crystal transition temperatures and phase textures were observed using polarizing optical microscope BIOLAR PI, equipped with the LINKAM 660 hot plate, controlled by the TMS 93 unit.

2.3. The Thermooptical Observations

Observation of the transmitted light intensity through the measuring cells placed in the birefractive set up were done upon slow cooling from isotropic state to the crystal one. Measurements were done with optical axis of the sample, defined in the SmC^* phase, oriented a few degree off the angle of maximum transmission.

Results are shown in the Figure 3. Sharp changes of the light intensity indicate phase transitions.

2.4. Tilt Angle

Tilt angles θ were studied by means of optical switching angle measurements. These electrooptical studies were performed for CO-20

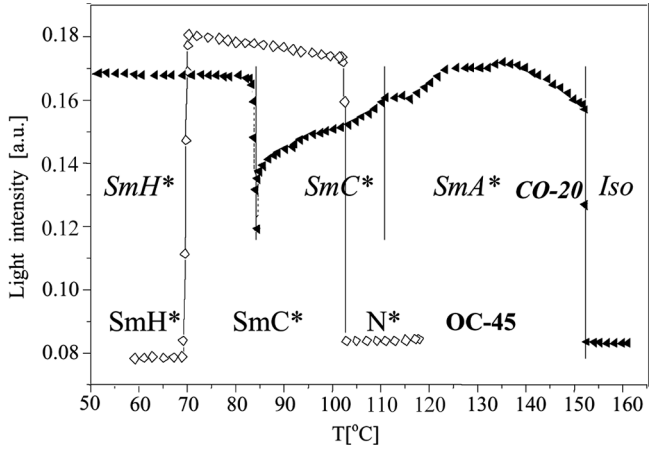

FIGURE 3 The intensity of the light transmitted through birefractive set up with studied (◂) CO-20 and (◇) OC-45 compounds upon cooling.

and OC-45 LCs. Results of these measurements are shown in the Figure 4.

2.5. Spontaneous Polarization

The spontaneous polarization P_s was evaluated from the integration of the depolarization current peaks in the same cell, as for the tilt angle measurements, under triangle electric pulse. The results of the P_s measurements are presented in the Figure 5.

2.6. X-Ray Diffraction Measurements

The smectic layer thicknesses as a function of temperature were obtained by Small-Angle X-ray Scattering (SAXS) experiments.

All measurements were done using HZG3 diffractometer with Cu lamp and Ni filter. The sample was placed on thermo-stabilized hot plate driven by UNIPAN 660 temperature controller. Samples were prepared by placing small amounts of studied compounds on the special scratched bar glass plates and heating them to isotropic phases. As a consequence, the free surface of the sample adopts homeotropic arrangement due to the surface action.

The internal diffraction maxima of SmA*, SmC* and SmH* phases were registered for full temperature ranges. These internal diffraction

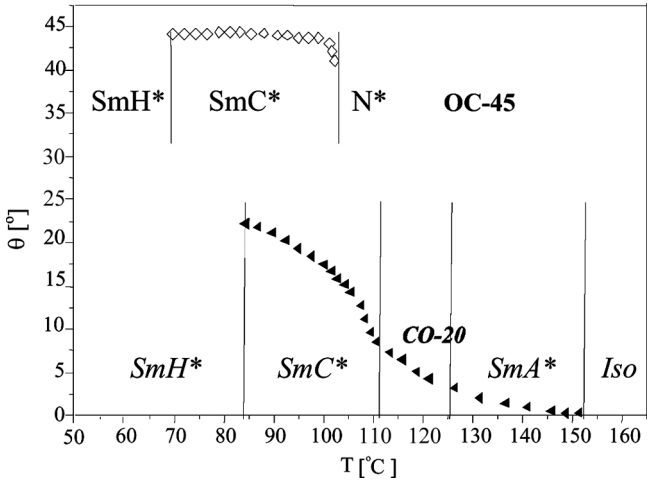

FIGURE 4 The tilt angle θ of (◂) CO-20 and (◇) OC-45 compounds measured at the temperature domain by optical switching method.

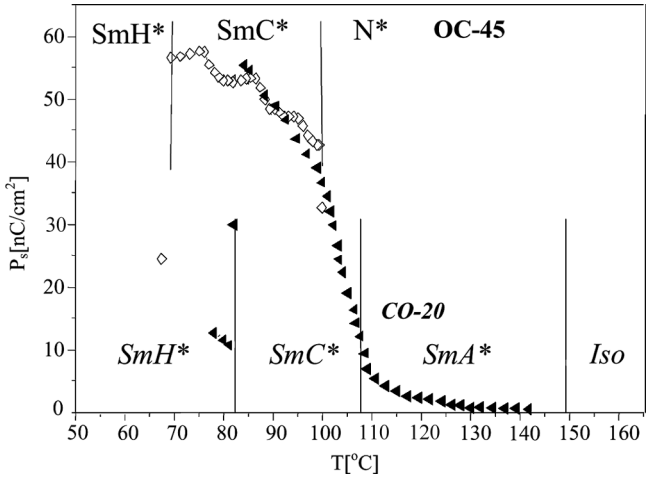

FIGURE 5 The spontaneous polarization P_s of the (◂) CO-20 and (◇) OC-45 compounds obtained by switching current method.

maxima were taken for calculations of smectic layer thicknesses using the Bragg law. At this point, it is worth noticing that apart from the main clear diffraction peak, the second one which is significantly smaller but distinct, was observed in all smectic phases (SmA*, SmC* and SmH*) of CO-20 and OC-45 compound (see Fig. 6). The calculated layer spacing d from our X-ray diffraction measurements are plotted in the Figure 7.

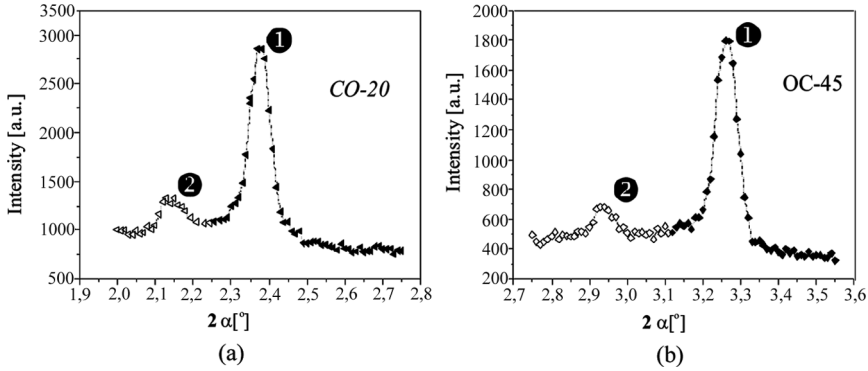

FIGURE 6 The powder SAXS spectrum of a) compound CO-20 and b) compound OC-45 in SmC* phases at T = 90 [°C].

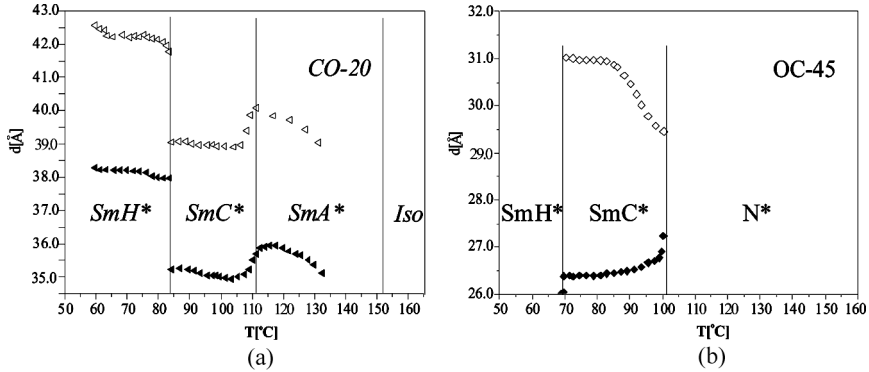

FIGURE 7 The layer spacing d versus temperature T of a) compound CO-20 and b) compound OC-45 obtained by SAXS measurements. Layer spacing d^1_{20} for CO-20 and d^1_{45} for OC-45 denoted by full figures (◄ and ◆) were calculated on the basis of main diffraction peaks ❶ (see Fig. 6) while the empty figures (◁ and ◇) correspond to layer spacing d^2_{20} and d^2_{45} obtained from the smaller ones ❷.

2.7. Switching Times

For the switching times studies measuring cells, described above, were used. The cells were placed in the birefractive set up and the switching times were measured under square electric filed pulse (E = 13 [V/μm]), upon cooling through whole temperature range of the SmC* phase.

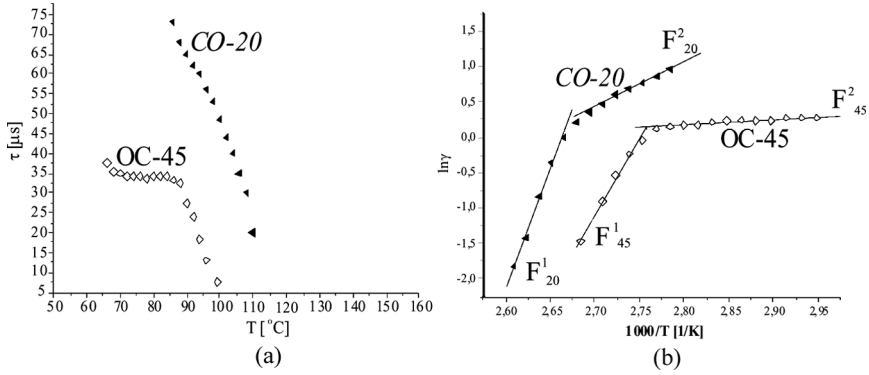

FIGURE 8 a) Switching times τ in SmC* phases versus temperature T for CO-20 (◄) and OC-45 (◇) under square electric filed pulse (E = 13 [V/μm]), b) The plot of ln(γ) versus 1000/T for CO-20 (◄) and OC-45 (◇) compounds.

The results of these measurements are presented in the Figure 8a. The switching time τ was measured as 80% of the time of full reorientation of the vector of spontaneous polarization P_s. Using relation (1):

$$\tau = \gamma \frac{1}{P_s E} \tag{1}$$

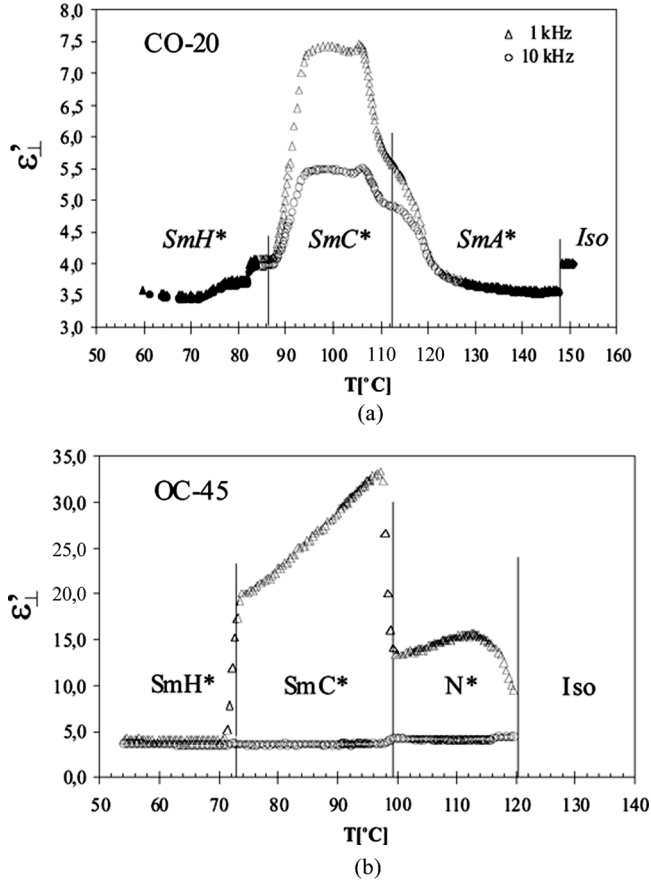

FIGURE 9 a) Temperature dependence of the real part of the perpendicular component of electric permittivity $\varepsilon'_\perp$ of CO-20 for two frequencies: △-1 [kHz] and ○-10 [kHz]. b) Temperature dependence of real part of the perpendicular component of electric permittivity $\varepsilon'_\perp$ of OC-45 for two frequencies △-0.1 [kHz] and ○-10 [kHz].

and knowing values of the spontaneous polarization P_s and electric filed strength E one can calculate the rotational viscosity γ. In the Figure 8b the plot of $\ln(\gamma)$ versus 1000/T was drawn.

2.8. Dielectric Properties

Dielectric properties of CO-20 and OC-45 were studied in Iso, N*, SmA*, SmC* phases, over the frequency range from 10 [Hz] to 12 [MHz] using HP 6425 and HP 4192 A analyzers.

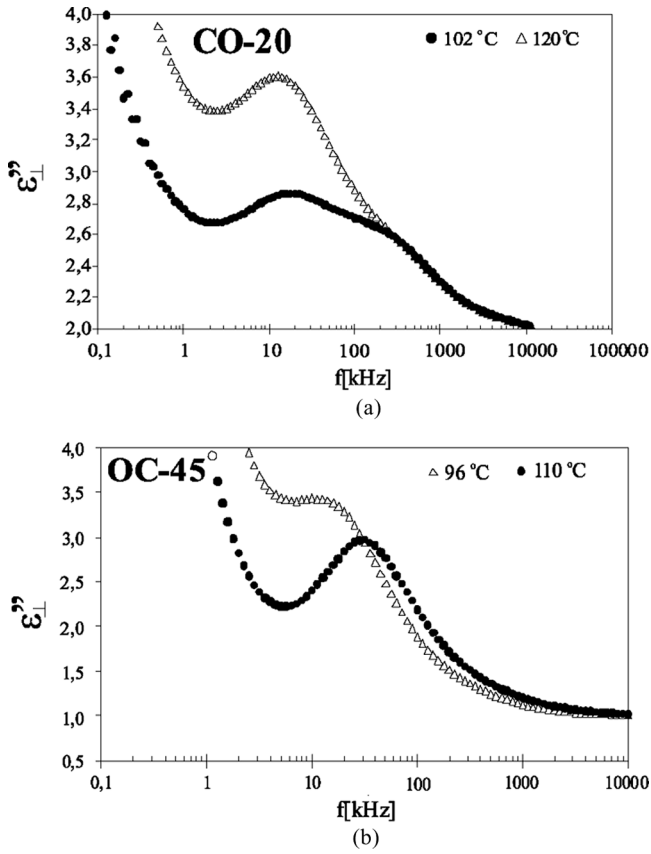

FIGURE 10 a) The imaginary part of the perpendicular component of electric permittivity $\varepsilon''_\perp$ versus frequency of the applied electric field of CO-20 for two temperatures: ●-T = 102 [°C] (in SmC* phase), △-T = 120 [°C] (in SmA* phase). b) The imaginary part of the perpendicular component of electric permittivity $\varepsilon''_\perp$ versus frequency f.

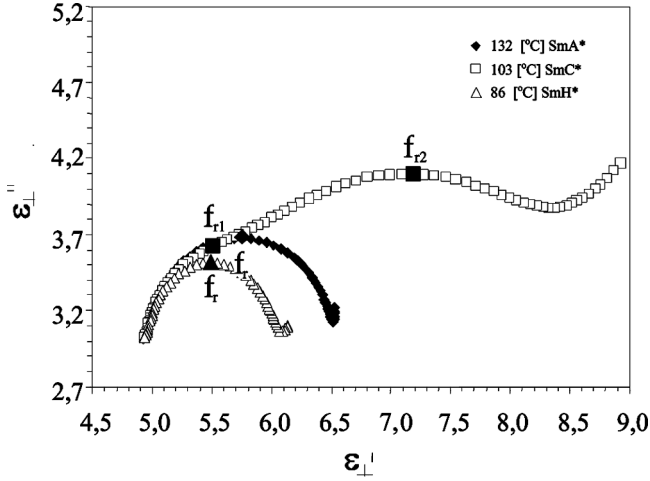

FIGURE 11 The Cole-Cole plot for CO-20 (◆) in the SmA* phase at T = 132 [°C] ($f_r = 178$ [kHz]); (□) in the SmC* phase at T = 103 [°C] ($f_{r1} = 125.3$ [kHz], $f_{r2} = 15.8$ [kHz]); (△) in the SmH* phase at T = 86 [°C] ($f_r = 316$ [kHz]).

For this study, the special cells were prepared in our laboratory and afterwards used. The cell gap varied from 1.5 to 20 [μm]. Chosen results are presented in Figures 9–11.

3. DISCUSSION AND CONCLUSIONS

Experiments described in the Chapter 2 combined with computer calculations show that:

1) The molecular lengths $l_{20} = 34.3$ [Å] and $l_{20}^m = 51.9$ [Å] of the CO-20 molecule are comparable to the lengths $l_{45} = 35.1$ [Å] and $l_{45}^m = 51.1$ [Å] of the OC-45 one (see Table 1 and Fig. 12).
2) The total dipole moment $\mu_{20} = 2.16$ [D] of CO-20 molecule is significantly smaller than $\mu_{45} = 2.60$ [D] for OC-45 molecule (see Table 1).
3) Vectors of both dipole moments $\vec{\mu}_{20}$ and $\vec{\mu}_{45}$ are nearly perpendicular to their long molecular axes of inertia (see Table 1).
4) Vectors of dipole moments, $\vec{\mu}_{20}$ characterized by $\varphi_{20} = -63^\circ$ and $\gamma_{20} = 90^\circ$ and $\vec{\mu}_{45}$ characterized by $\varphi_{45} = +50^\circ$ and $\gamma_{45} = 90^\circ$, are nearly opposite (see Table 1).
5) The compound CO-20 shows smectic phase only (SmA*, SmC*, SmH*), while in the OC-45 compound the chiral nematic phase (N*) appears before the smectic ones, SmC* and SmH* (see Table 2).

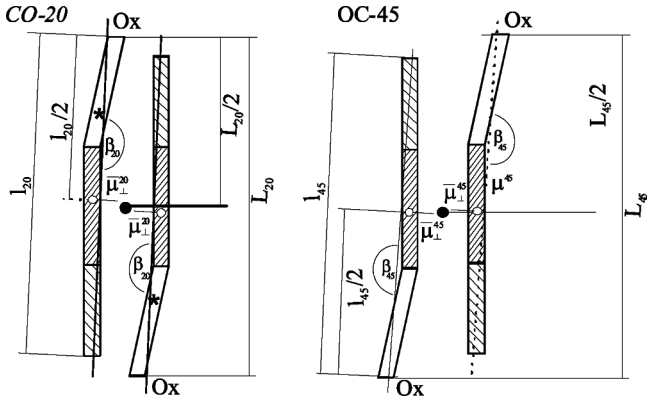

FIGURE 12 Mean virtual dimmers of two antiparallel CO-20 and OC-45 molecules. L_{20} stands for the total length of the objects in CO-20 and L_{45} is the total length of those for OC-45 compound. The centre of the molecule and the centre of the average object are denoted by figures ○ and ● respectively.

6) Please notice that SmA*–SmC* and SmC*–SmH* phase transitions in CO-20 as well as N*-SmC* phase transition in OC-45 are characterized by very small phase transition enthalpies ΔH (see Table 2).
7) The compound CO-20 saturates its tilt angle θ_{20} at approximately 20°, while the OC-45 compound, saturates its tilt angle θ_{45} at about 45°. In the case of compound CO-20 small tilt angle θ can be induced by E = 13 [V/μm] in the whole temperature range of the orthogonal SmA* phase (see Fig. 4).
8) Both the CO-20 and OC-45 materials exhibit almost the same saturated value of the spontaneous polarization P_s, while their

TABLE 2 Phase Transition Temperatures T_D [°C] and Enthalpies ΔH [kJ/mol] Determined by DSC and Phase Transition Temperatures T_M [°C] Determined by Optical Microscopy for the Compounds CO-20 and OC-45 Compounds

Molecule	SmH*	SmC*	SmA*	N*	Iso
CO-20	• 83.7	• 111.9	•	– 153.1	• T_D
	• 0.564	• 0.009	•	– 1.436	• ΔH
	• 84.0	• 111.0	•	– 151.0	• T_M
OC-45	• 79.0	•	−99.4	• 120.7	• T_D
	• 4.187	•	−0.669	• 0.303	• ΔH
	• 71.4	•	−102.4.0	• 120.7	• T_M

thermal characteristics are different. The spontaneous polarization of the OC-45 is almost temperature independent upon cooling through the SmC^* phase, while the spontaneous polarization P_s characteristic for the CO-20 material exhibits regular character. It is worth noticing that spontaneous polarizations P_s is measurable under electric field ($E \approx 13$ [V/μm]) within whole temperature range of SmA^* phase of CO-20. Moreover, the spontaneous polarization is measurable a few degrees Celsius above SmC^*–N^* phase transition, of compound OC-45 (see Fig. 5).

9) Layer spacing d_{20}^1 and d_{20}^2 obtained from SAXS measurements in all smectic phases of the CO-20 compound are higher than calculated adjacent molecular length l_{20} (see Fig. 7a).
10) Both later spacing d_{45}^1 and d_{45}^2 obtained from SAXS measurements in the tilted SmC^* phase of the OC-45 compound are smaller than calculated adjacent molecular length l_{45} but does not fit those calculated from the simple rigid-rod approximations $d_{45}^1 \neq l_{45} \cdot \cos\theta$ (see Fig. 7b).
11) Switching time τ_{45} of OC-45 is significantly smaller than τ_{20} of CO-20 measured in the SmC^* phase at the same temperature.
12) The rotational viscosity γ_{20} calculated from τ_{20}, P_s^{20} and E for CO-20 is significantly higher than rotational viscosity γ_{45} calculated from τ_{45}, P_s^{45} and E for OC-45 (see Fig. 8a).
13) It can be noticed that in Arhenius plots:

$$\ln\gamma = \ln A + \frac{F}{T_r} \tag{2}$$

where A is a constant, T_r is a reduced temperature, and F stands for an activation energy, drawn for both compounds (see Fig. 8b) in SmC^* two temperature ranges with different activation energies F^1 and F^2 are distinguished.
14) It is highly important that, apart from the main Goldstone modes in SmC^* phases (at small frequencies $f_r < 1$ [kHz]), one can observe another "Goldstone modes" not only in SmC^* but in SmH^*, SmA^* and even in N^* phases (with $f_r > 10$ [kHz], see Figs. 9 and 10).

Above differences in the physical properties between mesogenic compounds CO-20 and OC-45 can not be explained taking into consideration only properties of the single molecules. As far as the CO-20 compound is concerned:

a) the main layer spacing d_{20}^1, which corresponds to the smectic layer thickness, is higher than calculated molecular length l_{20} in both

SmA* and SmC* phases and the layer spacing change during SmA*–SmC* phase transition is insignificant,

b) SmA*–SmC* phase transition is characterized by very small phase transition enthalpy ($\Delta H = 0.009$ [kJ/mole]),

c) the optical tilt θ and the spontaneous polarization P_s can be easily induced in whole temperature range of the SmA* phase, which can not be considered as an electroclinic effect,

d) the Goldstone mode appears in the SmA* phase,

one can conclude that SmA* phase of CO-20, to some extend, follows the scheme proposed by de'Vries [5–7].

According to this model, the objects from which the SmA* phase is built up are already tilted with respect to the layer normal in SmA* phase. In the simple rod-like approximation the average length L_{20} of this objects in the SmA* phase is higher than molecular length l_{20}. Our preliminary computer simulations confirmed that two CO-20 molecules can build two possible kinds of antiparallel dimmers. Those dimmers are characterized by total lengths L^1_{20} and L^2_{20}. Molecules of OC-45 can form the dimmer with length L^1_{45} only. Furthermore, not only the SmA* phase consists of monomers with l_{20} and dimmers with L^1_{20} and L^2_{20} but SmC* and SmH* phases also. Therefore,

TABLE 3 The Results of Computer Calculations for CO-20 and OC-45

	CO-20			OC-45
	$l_{20} = 34.3$ [Å]; $L^1_{20} = 37.5$ [Å]; $L^2_{20} = 41.0$ [Å]			$l_{45} = 35.1$ [Å]; $L_{45} = 36.3$[Å]
Phase	SmH*	SmC*	SmA*	SmC*
T [°C]	75	88	120	95
d^1 [Å]	$d^1_{20} = 38.0$	$d^1_{20} = 35.3$	$d^1_{20} = 35.6$	$d^1_{45} = 26.8$
d^2 [Å]	$d^2_{20} = 42.0$	$d^1_{20} = 38.8$	$d^1_{20} = 39.5$	$d^2_{45} = 29.5$
θ^E	–	$\theta^E_{20} = 18°$	$\theta^E_{20} = 6°$	$\theta^E_{45} = 45°$
L [Å]	$L_{20} = 39.3$	$L_{20} = 37.5$	$L_{20} = 36.7$	$L_{20} = 35.7$
θ^T	$\theta^T_{20} = 18°$	$\theta^T_{20} = 22°$	$\theta^T_{20} = 16°$	$\theta^T_{45} = 46°$
d^{2T} [Å]	$d^{2T}_{20} = 42.9$	$d^{2T}_{20} = 38.4$	$d^{2T}_{20} = 38.0$	$d^{2T}_{45} = 27.3$

Spacing d^1 and d^2, the tilt angle θ^E are taken out of the experiment.
The dimmer length of L_{20} in SmA* was estimated as $L_{20} = \lfloor l_{20} + (L^1_{20} + L^2_{20})/2 \rfloor /2$.
The dimmer length of L_{20} in SmC* was estimated as $L_{20} = \lfloor l_{20} + L^1_{20} + L^2_{20} \rfloor /3$.
The dimmer length of L_{20} in SmH* was estimated as $L_{20} = \lfloor L^1_{20} + L^2_{20} \rfloor /2$.
The angle of θ^T in tilted SmH* phase of CO-20 was estimated as $\theta^T = \theta^E_{20}$.
The spacing of d^{2T}_{20} was estimated as $d^{2T}_{20} = d^1_{20} + (L_{20} - l_{20}) \cdot \cos\theta^T_{20}$.
The spacing of d^{2T}_{45} was estimated as $d^{2T}_{45} = d^1_{45} + (L_{45} - l_{45}) \cdot \cos\theta^T_{45}$.

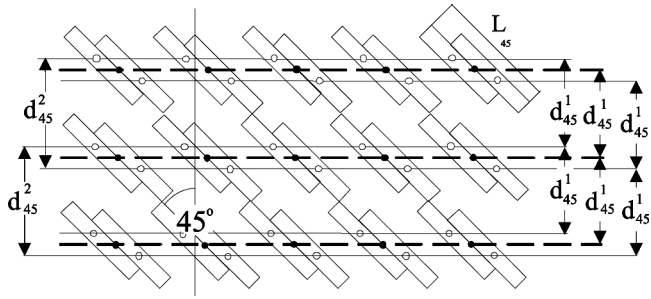

FIGURE 13 The structure of SmC* phase of OC-45 and the definition of parameters measured by SAXS – d^1_{45} and d^2_{45}. As one can see: $d^1_{45} = L_{45} \cdot \cos\theta$, but $d^2_{45} = d^1_{45} + (L_{45} - l_{45}) \cdot \cos\theta$.

the given phase of CO-20 may be described by the average object with average length L_{20}.

The Figure 12 shows the simplified scheme of such virtual objects for CO-20 and OC-45. In the Table 3 calculated characteristic lengths of those objects are gathered as well as tilts angles calculated using them.

To support the above hypothesis of the dimmers and monomers coexistence, let us notice that relaxation mechanism in the SmC* phase of CO-20 can be described by two higher relaxation frequencies $f_{r1} = 125.3$ [kHz], $f_{r2} = 15.8$ [kHz] (see Fig. 11) which are probably connected with vibrations of two types of objects mentioned above, with characteristic lengths L^1_{20} and L^2_{20}. Other evidence of existence of such objects are: significant change of values of activation energies from F^1 into F^2 upon temperature T decreases and apparent increase of d^2_{45} upon cooling in SmC* phase of OC-45. The Figure 13 explains the structure of the SmC* phase of OC-45 and defines parameters measured by SAXS–d^1_{45} and d^2_{45} (compare with Figs. 6 and 7). The similar structure can be be regarded to SmC* phase of CO-20 compound.

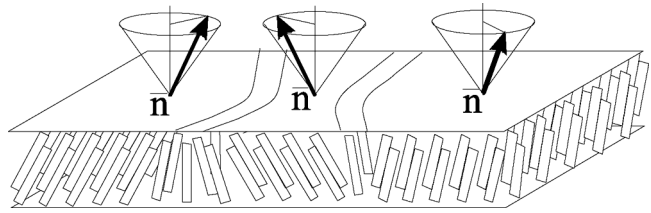

FIGURE 14 The structure of the de'Vries-like "block SmA_b" phase of the CO-20 compound.

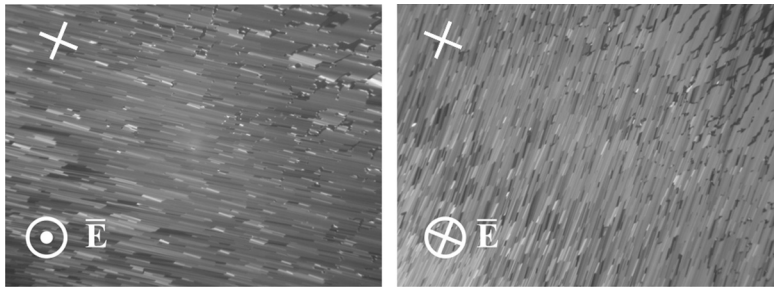

FIGURE 15 Microphotograms of SmC* phase induced from N* one of OC-45 compounds obtained using opposite direction of the electric field $\vec{E}$. The red cross denoted the orientation of the polarizer and the analyzer.

Our studies prove that the orthogonal SmA* of the CO-20 compound is rather build up with tilted crystallite like small pieces (blocs) of SmC*, having the common smectic planes and randomly oriented projection of their director on the smectic plane. So that, this block SmA* phase (SmA_b^*) is orthogonal and optically uniaxial. At the SmA_b*–SmC* phase transition the rotational symmetry of domains distribution is lost and the SmC* phase becomes tilted and optically biaxial. The following Figure 14 explains the structure of the de'Vries-like, block "SmA_b" phase of CO-20.

Presented investigations prove that the N* phase of OC-45, which easily transfers in to SmC* under electric field [3] and showing Goldstone mode, is built from smectic-like block with some spontaneous polarization P_s too. In the Figure 15 microphotograms of SmC* phase induced from N* one of OC-45 compound is shown. This SmC* phase induction was observed earlier by Anderson *et al.* [3].

Moreover, it seems that interlayer interactions in the SmC* of CO-20 are higher than those in OC-45, because biased rotation degree η must obey following relation $\eta_{45} \ll \eta_{20}$ under $P_s^{45} \approx P_s^{20}$ while $\theta_{45} gt; gt; \theta_{20}$ what was explained by us earlier [8–9]. The above statement, seems to be in the good agreement with observation that switching time τ_{45} of OC-45 is considerably smaller than τ_{20} of CO-20 measured in the SmC* phase at the same temperature.

REFERENCES

[1] Furukawa, K., Terashima, K., Ichihashi, M., Saito, S., Miyazawa, K., & Inukai, T. (1988). *Ferroelectrics*, *85*, 451.
[2] Skarp, K., Flatischer, K., & Lagerwall, S. T. (1988). *Ferroelectrics*, *84*, 183.

[3] Andersson, G., Flatischer, K., Komitov, L., Lagerwall, S. T., Skarp, K., & Stebler, B. (1991). *Ferroelectrics*, *113*, 361.
[4] Piecek, W., Raszewski, Z., Perkowski, P., Kędzierski, J., Rutkowska, J., Zieliński, J., Nowinowski-Kruszelnicki, E., Dąbrowski, R., Tykarska, M., & Przedmojski, J. (2005). *Molecular Crystals and Liquid Crystals*, *436*, 149.
[5] de Vries, A. (1979). *Journal of Chemical Physics*, *71*, 25.
[6] de Vries, A., Ekachai, A., & Spielberg, N. (1979). *Molecular Crystals and Liquid Crystals Letters*, *49*, 143.
[7] Lagerwall, J. P. F., Giesselman, F., Radcliffe, M. D. (2002). *The Physica Review*, *E66*, 031703.
[8] Raszewski, Z., Rutkowska, J., Kędzierski, J., Perkowski, P., Piecek, W., Zieliński, J., Żmija, J., & Dąbrowski, R. (1995). *Molecular Crystals and Liquid Crystals*, *263*, 271.
[9] Raszewski, Z., Rutkowska, J., Kędzierski, J., Perkowski, P., Piecek, W., Zieliński, J., Żmija, J., & Dąbrowski, R. (1997). *Molecular Crystals and Liquid Crystals*, *302*, 85.